iScience

Article

An evolutionarily conserved role for CTNNB1/β-CATENIN in regulating the development of the corpus callosum

Graphical abstract

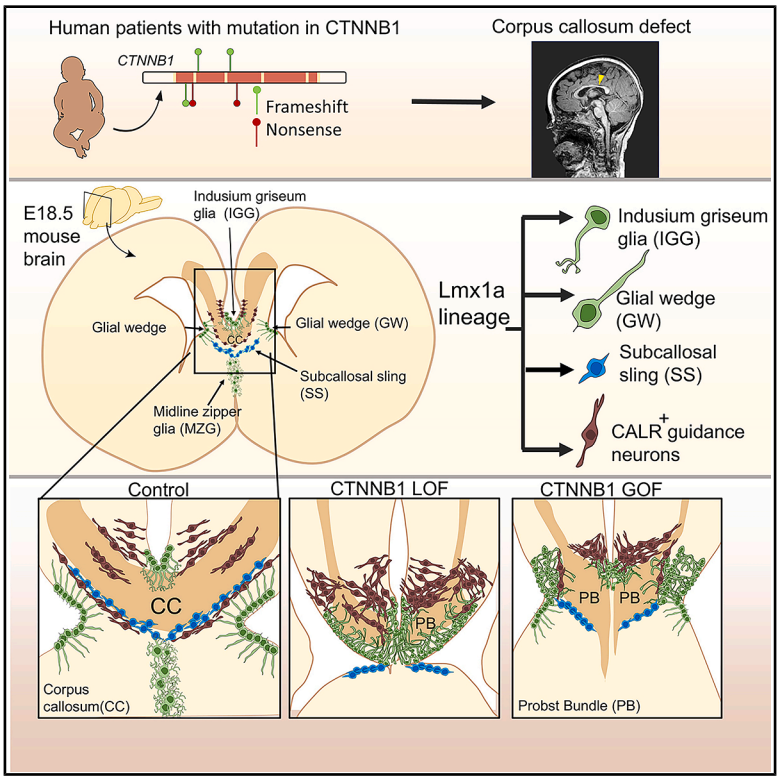

Highlights

- CTNNB1 gene mutations cause corpus callosum (CC) defects in humans
- Embryonic midline-specific gain or loss of function of CTNNB1 in mice disrupts CC crossing
- The Lmx1a lineage contributes to midline glial and neuronal CC guidance cell populations
- Lmx1a-lineage-derived CC guidance cells are disorganized upon CTNNB1 gain and loss of function

Authors

Arpan Parichha, Debarpita Datta, Amrita Singh, ..., David Gosar, Damjan Osredkar, Shubha Tole

Correspondence

stole@tifr.res.in

In brief

Neuroscience; Molecular neuroscience; Developmental neuroscience

Parichha et al., 2025, iScience *28*, 113335
September 19, 2025
https://doi.org/10.1016/j.isci.2025.113335

CellPress

iScience

CellPress
OPEN ACCESS

Article

An evolutionarily conserved role for CTNNB1/β-CATENIN in regulating the development of the corpus callosum

Arpan Parichha,[1,2,3] Debarpita Datta,[1] Amrita Singh,[1] Ishita Talwar,[1] Shreya Yadav,[2,3] Mahima Bose,[1] Varun Suresh,[1] Špela Miroševič,[4] Nina Žakelj,[5] David Gosar,[4] Damjan Osredkar,[5,6] and Shubha Tole[1,7,*]

[1]Department of Biological Sciences, Tata Institute of Fundamental Research, Mumbai 400005, India
[2]CSIR- Institute for Genomics and Integrative Biology, Mathura Road, Sukhdev Vihar, New Delhi 110025, India
[3]Academy of Scientific and Innovative Research (AcSIR), Ghaziabad 201002, India
[4]Department of Family Medicine, Medical Faculty Ljubljana, Ljubljana, Slovenia
[5]Department of Pediatric Neurology, University Children's Hospital, University Medical Centre, Ljubljana, Bohoričeva 20, 1525 Ljubljana, Slovenia
[6]Center for Developmental Neuroscience, Medical Faculty Ljubljana, Ljubljana, Slovenia
[7]Lead contact
*Correspondence: stole@tifr.res.in
https://doi.org/10.1016/j.isci.2025.113335

SUMMARY

The corpus callosum (CC) is a major nerve bundle that connects the two hemispheres of the brain. Dysgenesis of the CC is associated with neurodevelopmental disorders such as the CTNNB1 syndrome. We identified that five individuals carrying *CTNNB1* mutations displayed CC deficits. To explore CTNNB1/β-CATENIN-dependent mechanisms that regulate CC midline crossing, we examined mice with *Ctnnb1* gain of function (GOF) or loss of function (LOF) selectively targeted to the early embryonic central nervous system midline using an Lmx1aCre driver. We identify that the Lmx1a lineage contributes to midline cell populations known to regulate CC pathfinding: the glial wedge, the indusium griseum glia, and a population of midline glutamatergic neurons. We find that each of these structures are affected in both GOF and LOF embryos, resulting in a profound disruption of CC crossing and formation of Probst bundles. Thus, regulated β-CATENIN function in midline cell populations is critical for CC development, and its dysregulation may underlie the CC deficits associated with CTNNB1 syndrome.

INTRODUCTION

The corpus callosum (CC), a major nerve bundle in the mammalian brain that establishes communication between the two cerebral hemispheres, comprises millions of axons in humans.[1,2] The pathfinding of CC axons is a complex process along a convoluted route across two hemispheres that are initially physically separated. Therefore, this process has been the subject of extensive exploration, and multiple midline cell types have been identified to play structural or molecular guidance roles in CC crossing.[3–5] These include glial and neuronal populations: the midline zipper glia (MZG) that bring the two hemispheres together[6]; the glial cells of the indusium griseum (IGG) and the glial wedge (GW) that prevent the CC from being diverted dorsally or laterally[3]; the neuronal subcallosal sling (SS) that prevents CC axons from being diverted ventrally to the septum[4]; and calretinin (CALR)$^{+}$TBR1^{+} guidance neurons that are located above and below the CC at the midline that attract callosal axons to the midline.[7]

Dysgenesis of the CC has been implicated in several neurodevelopmental disorders, including autism.[8] Given the importance of the CC in normal brain function, it is critical to link clinical investigations that identify genetic mutations associated with CC malformations to a comprehensive mechanistic examination at the cellular and molecular levels using more tractable model systems. CC agenesis has been reported in the CTNNB1 syndrome, which is caused by mutations in the *CTNNB1* gene, classified as a category-1-autism-associated risk gene in the "SFARI gene" database (https://gene.sfari.org/database/human-gene/CTNNB1). *CTNNB1* encodes β-CATENIN, a protein with two distinct functions. At the cell membrane, it participates in cell adhesion as part of the CADHERIN complex,[9] and when translocated to the nucleus, it is a central mediator of canonical Wnt signaling.[10] Our study identifies that five patients reported to carry mutations in *CTNNB1* (ClinVar: https://www.ncbi.nlm.nih.gov/clinvar) also display malformations in the CC.

We sought to explore this phenotype further in a mouse model. We discovered that each midline cell population implicated in the guidance of the CC, except the MZG, contains a partial contribution from the Lmx1a lineage. We used an Lmx1aCre driver[11] together with β-CATENIN gain-of-function (GOF) and loss-of-function (LOF) lines to examine the

A

Patient id	Clinical Variants	Domain location	Mutation type	Description of Corpus callosum defect
ID_148	c.680dup; p.Leu229Thr	ARM 2	Frame shift_dup	Abnormal morphology of the splenium of the corpus callosum is observed, which appears stocky and curved.
ID_165	c.703G>T; p.G235Ter	ARM 3	Nonsense	Shortened aspect of the corpus callosum.
ID_156	c.776del; p.Leu259Pro	ARM 3	Frame shift_del	Volumetric and diameter decrease of the posterior segment of the corpus callosum
ID_179	c.976 _979delAATA; p.Asn326	ARM 5	Frame shift_del	Slightly diffusely thinned corpus callosum, with tendency to dysmorphic appearance in its posterior third.
ID_192	c.1014G>A; p.Trp338Ter	ARM 5	Nonsense	Corpus callosum hypoplasia.

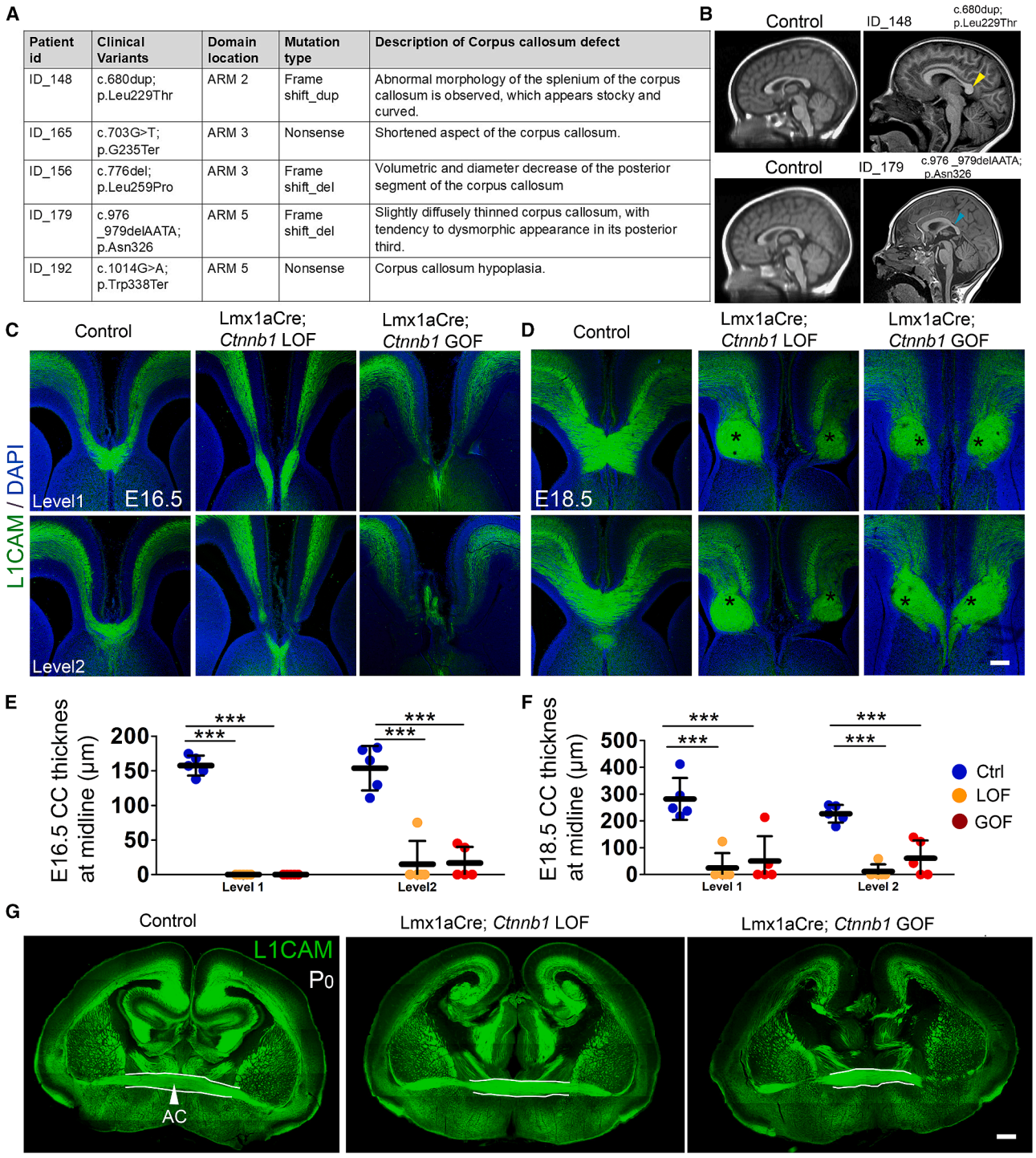

Figure 1. CC crossing defects in CTNNB1 syndrome patients and the *Ctnnb1* LOF and GOF mouse brains

(A) Table describing the CC phenotypes identified in brain MRI scans of five patients in the CTNNB1 syndrome patient cohort.

(B) Representative MR images of two patients with age-matched controls showing corpus callosum defect (arrowheads).

(C and D) Representative z-stacked confocal images of control, *Ctnnb1* LOF, and GOF mouse brains at E16.5 (C) and E18.5 (D) stained with L1CAM. Both *Ctnnb1* LOF and GOF brains display profoundly defective crossing of the CC and Probst bundles on either side of the midline (asterisks).

(legend continued on next page)

regulatory functions of CTNNB1 in CC crossing.[12,13] We report a striking agenesis of the CC in both CTNNB1 GOF and LOF conditions. We identify that altered CTNNB1 function causes severe disruption of the organization of the IGG, GW, and an increase in the number of Lmx1a-lineage-derived CALRT$^+$TBR1$^+$ midline neurons. Our findings provide a cellular-level mechanism that may potentially contribute to the CC dysgenesis component of CTNNB1 syndrome.

RESULTS

CC abnormalities in CTNNB1 syndrome patients

As part of a genotype-phenotype study on patients with CTNNB1 neurodevelopmental syndrome (ClinicalTrials.gov NCT04812119), five patients were identified to display an abnormal CC morphology based on analysis of their MRI scans. Genome sequencing revealed three patients to have frameshift mutations (c.680dup; p.Leu229Thr, c.776del; p.Leu259Pro, and c.976 _979delAATA; p.Asn326), whereas two patients have a nonsense mutation (c.703G>T; p.G235Ter and c.1014G>A; p.Trp338Ter) within an ARM repeat of the *CTNNB1* gene (Figure 1A; Figure S1). Four of these mutations had previously been reported as pathogenic variants of *CTNNB1* in the ClinVar database (https://www.ncbi.nlm.nih.gov/clinvar), and in this study, we report their association with abnormalities in the corpus callosum. Examples of MR images of two of these patients and age-matched unaffected individuals are in Figure 1B.

CTNNB1 LOF and GOF mouse models display profoundly defective CC development

We examined whether *Ctnnb1* GOF or LOF also affects the CC in the mouse. We used an Lmx1aCre line to target the cells in telencephalic midline from the earliest stages of neural tube formation,[11] together with two well-described floxed *Ctnnb1* mouse lines that either disrupt (LOF)[13] or stabilize (GOF)[12] β-CATENIN upon Cre-mediated recombination. LOF is due to the deletion of exons 2–6 of the *Ctnnb1* gene, leading to the production of a truncated form of CTNNB1, which is ultimately degraded.[13] Exon 3 of *Ctnnb1* gene encodes a region containing sites at which CTNNB1 is phosphorylated by GSK3β, typically leading to its degradation. GOF is achieved by deletion of exon 3 due to Cre-mediated recombination, resulting in a stabilized constitutively active form of CTNNB1 that can no longer be degraded.[12,14] We examined *Ctnnb1* LOF and GOF brains at two developmental time points, embryonic day 16.5 (E16.5), when CC crossing has begun, and E 18.5, when it is complete. Immunostaining for L1CAM, an adhesion molecule enriched in axonal tracts, reveals a near-complete failure of CC crossing at the midline in both *Ctnnb1* LOF and GOF brains (Figures 1C–1F; Figures S2A–S2C and S3). Instead, callosal axons form Probst bundles consisting of fibers that are unable to cross and remain at the midline (Figures 1C–1F; Figures S2A–S2C and S3). Notably, the anterior commissure, another major nerve tract connecting two hemispheres, remains intact in both *Ctnnb1* LOF and GOF brains (Figure 1G). These findings motivated a careful examination of the midline guidance cell populations arising from the Lmx1a lineage.

The Lmx1a lineage contributes partially to the midline guidance cell population necessary for CC crossing

We used a stop-floxed tdTomato reporter line (Ai9) to examine the Lmx1a lineage at E18.5. The GW and the IGG contained a substantial contribution from this lineage, such that 44% ± 8% and 33.4% ± 6% of the GFAP$^+$ cells were also Ai9$^+$ in the GW and the IGG, respectively (Figures 2A–2F; Figures S4A–S4I and S5A–S5E). The MZG population, however, did not appear to have any detectable contribution from the Lmx1a lineage (Figures S6A and S6B). Among the neuronal populations, the SS contained a minor contribution from the Lmx1a lineage, such that 4.5% ± 0.7% of the NeuN$^+$ cells were also Ai9$^+$ (Figures S6C–S6F). The CALRT$^+$TBR1$^+$ neurons positioned at the margin of the cingulate cortex and the cortico-septal boundary also contained a small contribution from the Lmx1a lineage (Figures 2G–2K; Figures S7A–S7D). In the cingulate cortex cluster, 9.9% ± 1% of the CALRT$^+$ and 10.47% ± 1.3% of the TBR1$^+$ cells were also Ai9$^+$. In the cortico-septal boundary cluster, 5.2% ± 1.2% of the CALRT$^+$ and 6.3% ± 1.7% of the TBR1$^+$ cells were also Ai9$^+$ (Figure 2K; Figure S7D). Additionally, a small fraction of neurons in the cingulate cortex that project their axons through CC are also derived from Lmx1a Lineage (Figures S8A–S8D). Collectively, we describe these Lmx1a-lineage-derived cells as "midline Lmx1a lineage cells."

The neuroepithelial progenitor domain of the midline Lmx1a lineage cells display active canonical Wnt signaling

We examined the midline progenitor domain located just above the septum in the rostral midline at E13.5 (Figures 3A–3H). *In situ* hybridization confirmed that the Lmx1aCre-driven Ai9 reporter domain closely matches the endogenous Lmx1a expression pattern (Figures 3B and 3D[14]) and overlaps with the glial marker brain lipid-binding protein (BLBP) (Figures 3C–3H). Additionally, we verified that this domain expressed SOX9 and β-CATENIN (Figures 3I–3M), suggesting a possible role for β-CATENIN in the development of these cells. Canonical Wnt target genes *Axin2* and *Lef1* were expressed in this progenitor domain at E13.5 and E15.5 (Figures 3N–3Q). Collectively, these findings indicate that canonical Wnt signaling is active in midline progenitors derived from the Lmx1aCre lineage. In the subsequent sections, we focused on the glial and neuronal components of the midline Lmx1a lineage cells and examined their development in *Ctnnb1* LOF and GOF brains.

(E and F) Scatterplot showing quantification of CC thickness in the midline at E16.5 (E) and E18.5 (F). Data represent mean ± SEM, and individual dots in the scatterplot represent biological replicates.

(G) L1CAM immunostained sections at P0 show that the anterior commissure (AC) is unaffected in the *Ctnnb1* LOF and GOF mouse brains. Statistical test: two-way ANOVA followed by Bonferroni post-test; $p < 0.0001$; $^*p < 0.05$; $^{**}p < 0.01$; $^{***}p < 0.001$; ns if p value >0.05. For (E–G), $N = 5$ brains (biologically independent replicates) examined over five independent experiments. Scale bars, 100 μm for all images in (C, D, and G).

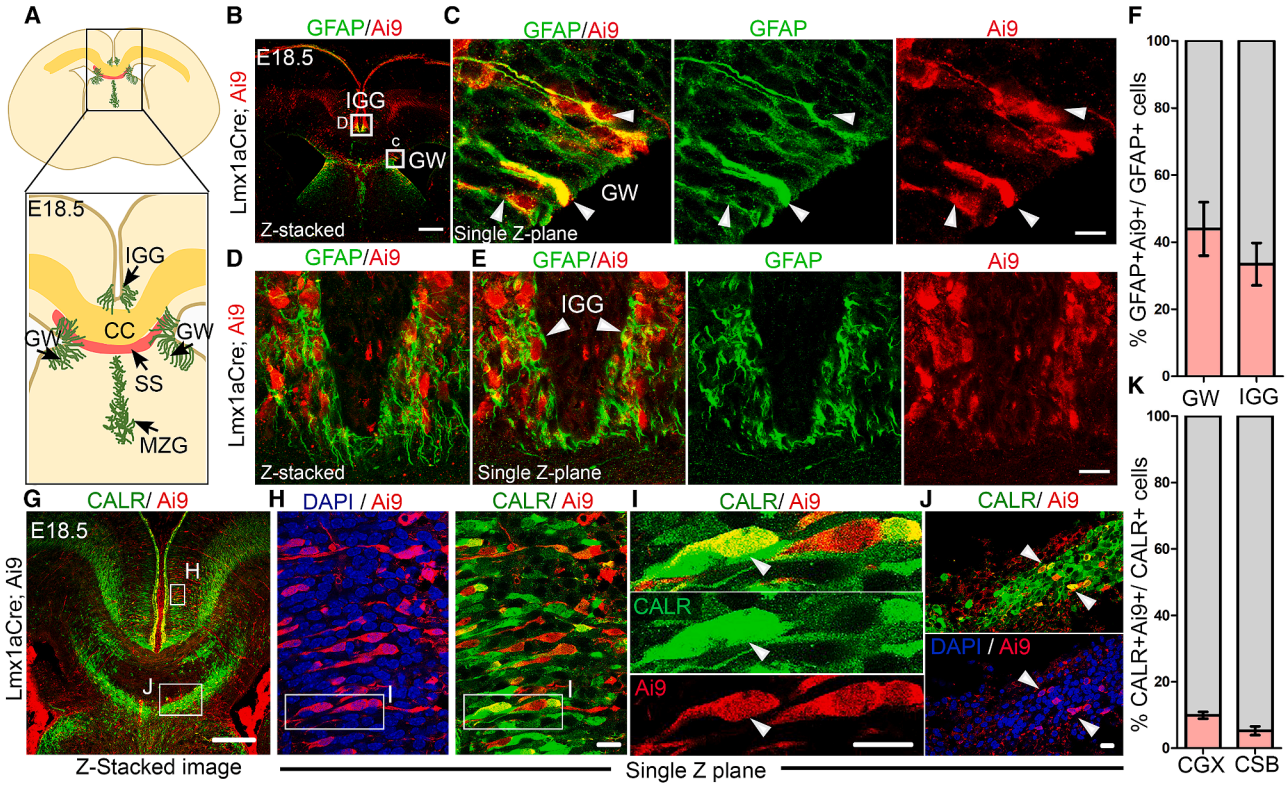

Figure 2. The Lmx1a lineage contributes to a subset of various cell types that guide CC crossing

(A) Cartoon showing the different midline guidance cell population that regulate CC crossing.

(B, D, and G) Representative z-stacked images of the E18.5 midline and (C, E, H, I, and J) single Z-planes showing the Lmx1a lineage in the GW (arrowheads, C), the IGG (arrowheads, E), and in the CALR$^+$ neurons in the cingulate cortex (CGX, H, I) and cortico-septal boundary (CSB, J) (arrowheads I and J).

(F and K) Quantification of the Lmx1a lineage; graphs represent mean ± SEM. The fraction of GFAP+ cells that are also Ai9+ is 44% ± 8% (GW) and 33.4% ± 6% (IGG), and the fraction of CALR+ cells that are also Ai9+ is 9.9% ± 1% (CGX) and 5.2% ± 1.2% (CSB). For (B–J), $N = 3$ brains (biologically independent replicates) examined over three independent experiments. The boxed area in (B and G) is shown at high magnification (mag) in (C, D and H, J), respectively; the boxed area in H is shown at high mag in I. Scale bars, 100 μm (B & G), 10 μm (C, E, H, I, and J).

CTNNB1 regulates the organization of the glial cells from the midline Lmx1a lineage

We examined the glial components of the midline Lmx1a lineage cells, the IGG and GW in *Ctnnb1* LOF and GOF brains at stages before (E15.5) and after (E18.5) CC crossing (Figures 4A–4H). In both LOF and GOF brains, there was a gross disruption of the organization of glia in these structures compared with controls (Figures 4C–4I; Figures S9A–S9C). At E15.5, the pioneering axons of cingulate neurons followed by isocortical neurons, follow a trajectory toward the midline, and at E16.5 they cross to the contralateral hemisphere.[1] We visualized midline glia using immunohistochemistry for ALDH1L1 and GFAP, the well-established markers for astroglial cells. In both LOF and GOF brains, ALDH1L1$^+$Ai9$^+$ or GFAP$^+$Ai9$^+$ midline glia appear disorganized compared to controls. By E18.5, when control callosal axons have crossed the midline, *Ctnnb1* LOF and GOF brains display Probst bundles encircled by GFAP$^+$Ai9$^+$ cell processes (arrowheads, Figures 4E and 4F; Figures S9A and S9B). These results suggest that misoriented and dysmorphic midline glial cells impair axonal guidance across the midline in *Ctnnb1* LOF and GOF brains.

A novel marker that distinguishes the IGG from the GW

The midline glial populations have been examined in the literature using standard glial markers, e.g., GFAP, BLBP, and GLAST.[3,5] However, there is a dearth of markers that distinguish the IGG from the GW, and selective markers for the IGG have not been identified. We analyzed a publicly available single-cell transcriptomic dataset,[15] which profiles the embryonic mouse cortex at postnatal day 0. The authors' original cell-type annotation identified two clusters as "Astrocytes (immature) 1 [10-P]" and "Astrocytes (immature) 2 [13-P]" (Figure 5A; Figure S10). We examined the distribution of established glial cell markers in these two clusters (Figures 5B–5E). The distribution of cells expressing *Fabp7* showed a sharp peak at a high (normalized) expression and a few cells at zero expression. This indicates that the majority of the cells examined express high levels of *Fabp7*, consistent with this gene being a pan-astrocyte marker. As expected, *Actb*, encoding β-ACTIN, displayed a similar expression profile since it is expected to be ubiquitous. In contrast, for *Aqp4* and *GFAP*, a large number of cells displayed zero expression, and others displayed a range of (normalized) expression values, indicating that these genes are not uniformly

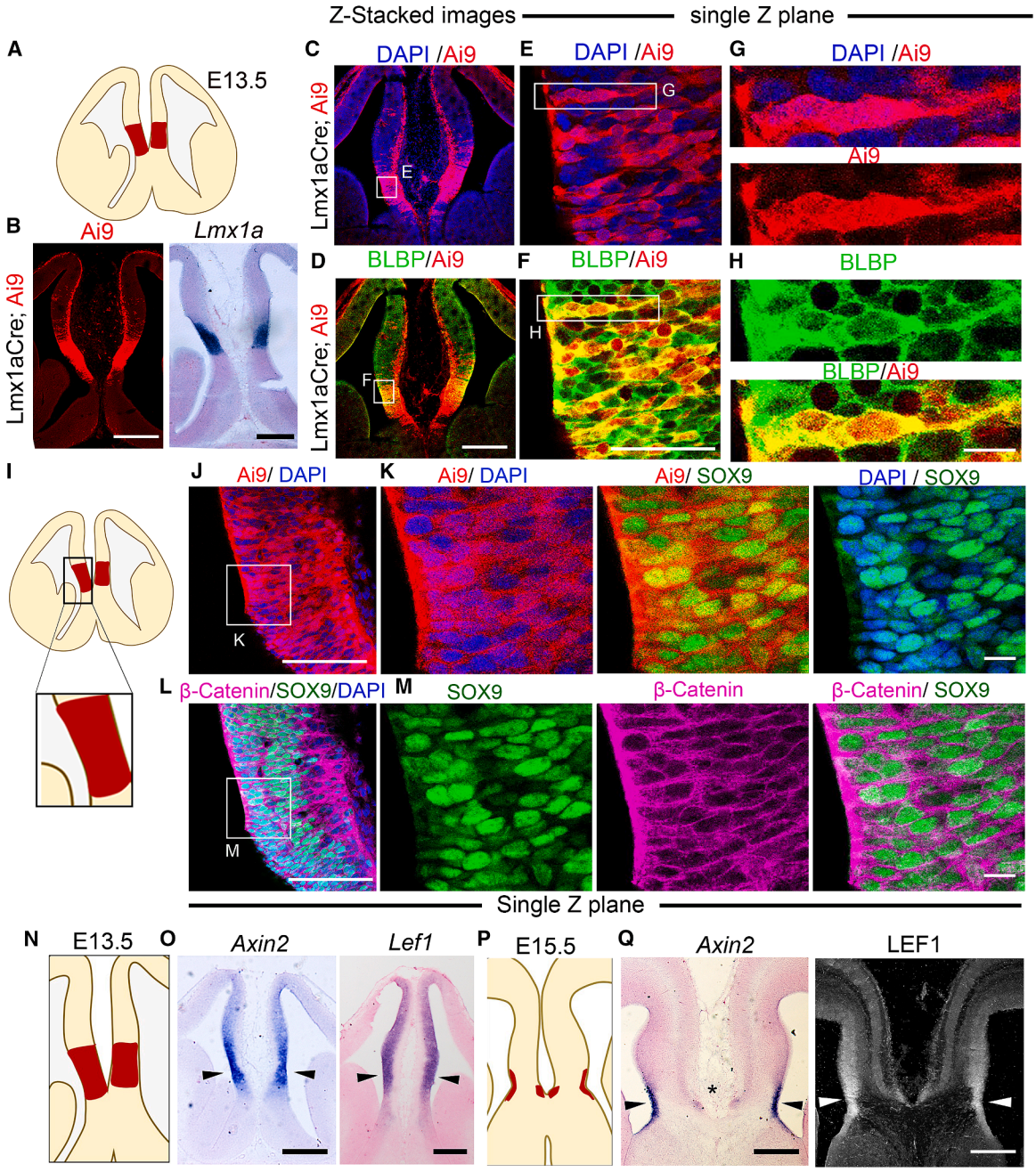

Figure 3. Canonical Wnt signaling components are present in the Lmx1aCre$^+$ midline progenitor domain

(A, I, and N) Cartoon showing the Lmx1aCre$^+$ progenitor domain at E13.5 and E15.5.

(B) Serial sections showing Lmx1aCre-driven Ai9 and *in situ* hybridization for endogenous *Lmx1a* mRNA.

(C, D, J, and L) Representative z-stacked low-mag images with single Z-planes of the boxed regions shown in adjacent panels (C->E; D->F; J->K; L->M). The boxed regions in (E and F) are shown at high mag in (G and H), respectively. The Ai9+ progenitor is BLBP$^+$ (C, D) and SOX9$^+$β-Catenin$^+$ (J, L).

(O) *Axin2* and *Lef1* mRNA are expressed in the midline progenitors at E13.5 (arrowheads).

(P and Q) At E15.5, a cartoon depicts the midline guidance populations that express *Axin2* mRNA and display LEF1 immunostaining (arrowheads, Q). For (A–Q), $N = 3$ brains (biologically independent replicates) examined over three independent experiments. Scale bars, 100 μm (B, C, D, O, and Q), 50 μm (F, J, and L), 10 μm (G, H, K, and M).

expressed in P0 astrocytes. Immunohistochemistry for AQP4 reveals that it marks cells located in the IGG but not the GW at E18.5 (Figure 5F), and these cells are also GFAP+ (Figures S11A and S11B). Upon *Ctnnb1* LOF or GOF, there was a significant increase in AQP4$^+$ cells in the IGG region (Figures 5F and 5G).

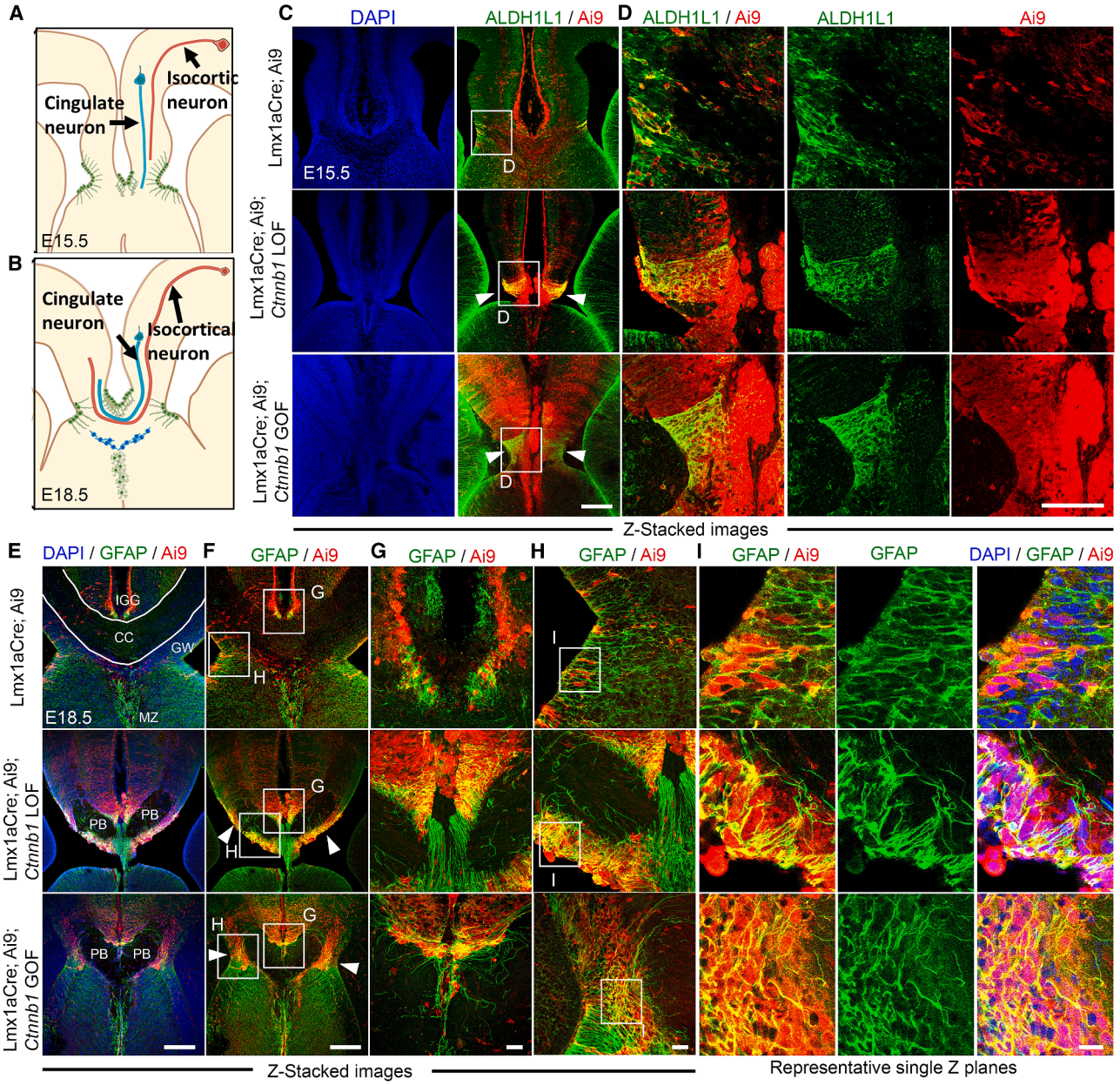

Figure 4. The organization of Lmx1a-lineage-derived ALDH1L1$^+$ GFAP$^+$ midline glial population is disrupted in *Ctnnb1* LOF and GOF brains

(A and B) Schematic representation of two developmental time points during CC formation: at E15.5, pioneer neurons from the cingulate cortex extend axons toward the septum, forming an initial trajectory that isocortical neurons follow but have not yet crossed the midline at that time; by E18.5, both cingulate and isocortical axons have successfully crossed the midline.

(C and D) Representative low- and high-mag z-stacked confocal images showing mispositioned ALDH1L1$^+$Ai9$^+$ midline glia in both *Ctnnb1* LOF and GOF brains compared with controls at E15.5. (D) High mag of the boxed regions in adjacent panels in (C).

(E and F) Representative low mag z-stacked confocal images showing disorganization of the GFAP$^+$Ai9$^+$ midline glial population in *Ctnnb1* LOF and GOF brains compared with controls at E18.5. (arrowheads, F).

(G and H) High-mag z-stacked images showing the boxed regions in adjacent panels in (F).

(I) High-mag single Z-planes showing boxed regions in adjacent panels in (H). For (C–I), *N* = 3 brains (biologically independent replicates) examined over three independent experiments. Scale bars, 100 μm (C, E, and F), 50 μm (D), 10 μm (G–I).

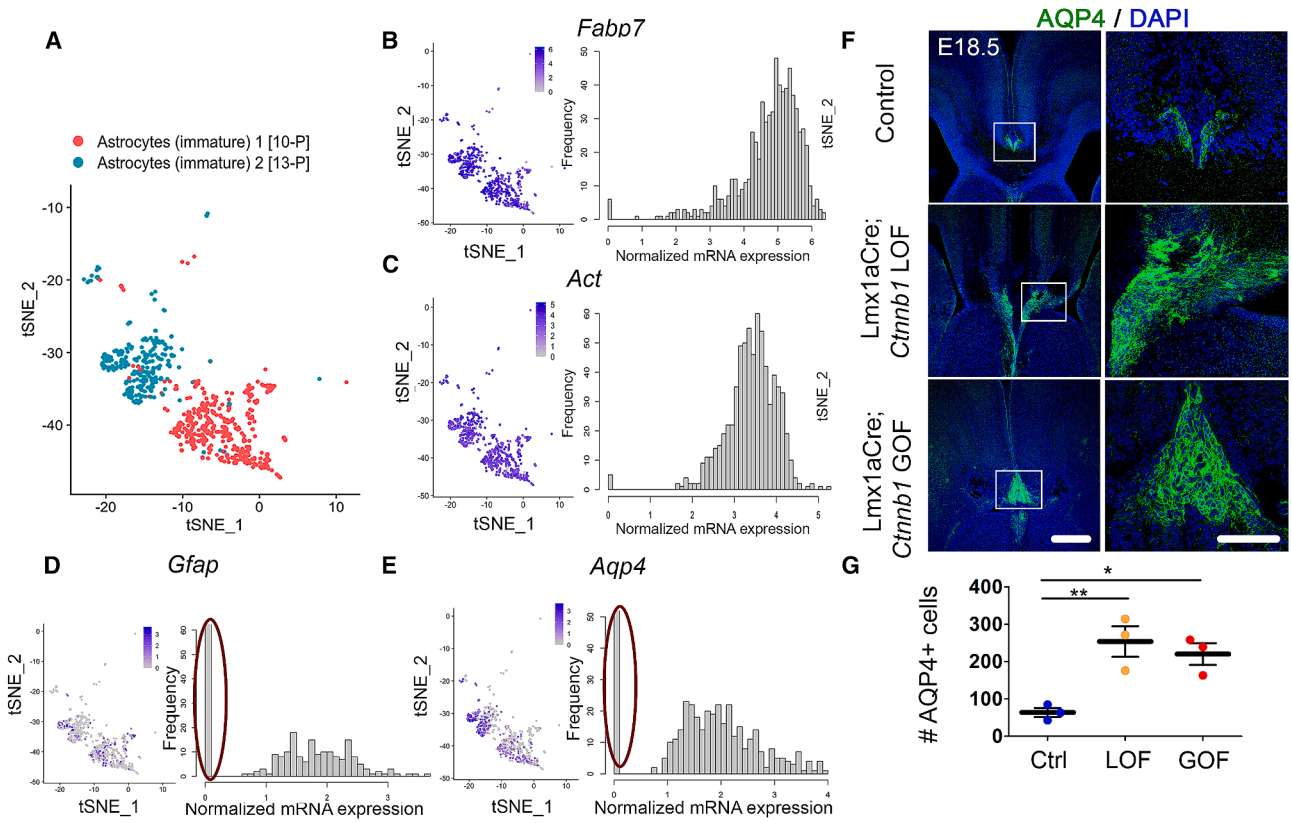

Figure 5. Analysis of publicly available single-cell RNA seq data reveals markers differentially expressed in glial populations and highlights the defects in *Ctnnb1* LOF and GOF mouse brain

(A) t-SNE plot of the astrocyte clusters from the publicly available scRNA-seq dataset from Loo et al. 2019, which profiles the embryonic mouse cortex at postnatal day 0.

(B–E) Heat maps and histograms show the distribution of known glial markers across postnatal astrocytes. Red ovals (D and E) indicate a large number of cells at expression level 0.

(F and G) Immunostaining for Aqp4 (F) and quantification (G) reveals an increased number of AQP4$^+$ IGG in the *Ctnnb1* LOF & GOF brains at E18.5, graphs represent mean ± SEM. Statistical test: 1 way ANOVA followed by Dunnett's multiple comparison test; $p < 0.0001$; $^*p < 0.05$; $^{**}p < 0.01$; $^{***}p < 0.001$; ns if p value >0.05. For E–G, $N = 3$ brains (biologically independent replicates) examined over three independent experiments. Scale bars, 50 μm for all images.

CTNNB1 regulates the distribution of midline CALR$^+$, TBR1$^+$ cells

We examined CALR$^+$, TBR1$^+$ cells, the major neuronal components of the midline Lmx1a lineage, and their development in *Ctnnb1* LOF and GOF brains. At E18.5, these neurons are arranged in three distinct bands: above, below, and within the CC (arrowheads, Figure 6A; Figure S12). In both *Ctnnb1* LOF and GOF brains, the overall organization of these CALR$^+$ bands appeared to be disrupted, such that these neurons no longer appeared in three distinct stripes (dashed ovals, Figure 6A; Figure S12). This indicates that CTNNB1 regulates the overall organization of the midline Lmx1a lineage CALR$^+$ neurons, which guide the CC crossing.

DISCUSSION

Guidance of the CC axons through the sharp turn they must take to enter the contralateral cortex requires the concerted action of multiple neuronal and glial cell populations.[3,4,6] CTNNB1/β-CATENIN has multiple roles in cortical neuroepithelial stem cells.[16] The dorsal telencephalic midline expresses multiple canonical Wnt ligands[14,17] and components of Wnt signaling, including CTNNB1. Together with the observation of CC deficits in CTNNB1 syndrome patients, this motivated the examination of CTNNB1 in the guidance of the CC using a mouse model.

In our mouse model, the *CTNNB1* LOF and GOF perturbation is selective to the midline guidance population that arises from the Lmx1a lineage. We identify that this lineage contributes to a subset of midline guidance cells, including both glial and neuronal population. We find that both the *Ctnnb1* LOF and GOF brains exhibit a major disruption in CC crossing, despite the Lmx1a lineage being only a partial contributor to the midline guidance populations. In contrast, the anterior commissure is unaffected in *CTNNB1* LOF and GOF brains. This is likely due to the fact that the MZG population does not include any detectable contribution from the Lmx1a lineage. This population is critical in mediating fusion of the ventral telencephalon/septum area, which is in turn necessary for crossing of the anterior commissure.[18] That the anterior commissure is unaffected in *Ctnnb1* LOF or GOF brains provides a useful internal control.

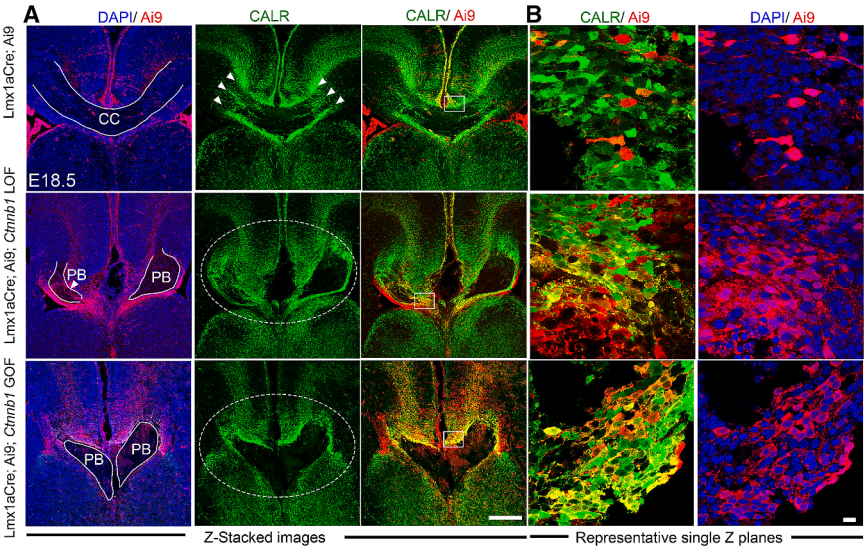

Figure 6. The organization of Lmx1a-lineage-derived CALR+ neurons around the midline is disrupted in *Ctnnb1* LOF and GOF brains

(A) Low-mag representative confocal z stacks show three bands of CALR+ neurons in the control midline (arrowheads) and their disorganized appearance in the LOF and GOF brains (dashed ovals).

(B) High-mag single Z-planes corresponding to the boxed regions in the adjacent panels in (A). N = 3 brains (biologically independent replicates) examined over three independent experiments. Scale bars, 100 μm (A), 10 μm (B).

Our findings, therefore, bring a precise cell-type-level understanding to a commissural crossing phenotype previously described for *Ctnnb1* LOF using the pan-dorsal telencephalic D6 Cre, which acts in the neocortical neurons projecting via the CC as well as all cells originating from dorsal telencephalic progenitors.[19]

Since *Ctnnb1* is implicated in both canonical Wnt signaling and cell adhesion, it is possible that either or both functions are important for the proper development of the GW and IGG cells. Mutations in several components of the Wnt/β-catenin signaling pathway are associated with CC defects in mice and humans.[20] In mice, mutants for Wnt receptor *Fzd3* exhibit CC crossing defects,[21] and mutants for the non-canonical Wnt signaling receptor Ryk display delayed and aberrant CC crossing.[22] WLS (Wntless), which regulates the secretion of Wnt ligands, was shown to be crucial for CC crossing.[23] A subset of patients with mutations in the *WLS* gene also display hypoplasia of the CC.[24] MRI data from patient cohorts with *APC2* mutations show thinning of the CC,[25] and patients carrying *de novo* mutations in the *CTNNB1* gene also show defects in the CC.[20] These defects may be consistent with a transcriptional role for CTNNB1 in callosal neurons.

However, we find that either gain or loss of function of *Ctnnb1* in the Lmx1aCre lineage leads to very similar CC crossing phenotypes. Since bidirectional regulation of downstream targets is unlikely to result in similar phenotypes, rather, dysregulation of cell adhesion may explain these findings. If the midline lineages arising from Lmx1aCre-driven LOF or GOF are disrupted in terms of cell adhesion, it is expected that this would result in dysmorphic organization, which would in turn have non-cell-autonomous consequences on midline axon crossing. Supporting this interpretation, mouse mutants harboring a Thr653lys substitution in an Armadillo repeat of *CTNNB1* display alterations in cell-cell adhesion properties and also defective CC crossing.[26]

Wnt/β-catenin signaling can crosstalk with different signaling pathways to regulate the organization of the midline guidance populations. Previous reports suggest that the Hedgehog signaling pathway regulator Gli3 coordinates with Fgf and Wnt/β-catenin signaling to regulate midline glial architecture.[27] This evidence motivates further investigation to identify the signaling molecules that are upstream or downstream to *CTNNB1* that mediate the function of CTNNB1 in the development of the complex cell populations that guide CC crossing at the midline.

Limitations of the study

CTNNB1 syndrome is a monogenic disorder caused by *de novo* germline mutations that impair one copy of the *CTNNB1* gene, which may result in reduced or increased CTNNB1 protein function depending on the nature of the mutation. In contrast, our *Ctnnb1* LOF model results in gene disruption of both copies and loss of all CTNNB function. We do not find a CC phenotype in Lmx1aCre; *Ctnnb1 loxP*/+ mice, indicating that the threshold requirement for CTNNB1 for CC crossing is met in heterozygote mice. The GOF model produces one allele that encodes a constitutively stabilized CTNNB1 protein, whereas the human mutations may result in one that is only partially stabilized. Mouse models that result in partially reduced or increased CTNNB function may recapitulate the human CTNNB1 syndrome better. Furthermore, mice in which either the transcriptional or the cell adhesion function of CTNNB1 has been selectively disrupted[28,29] would clarify the role of CTNNB1 in the Lmx1a midline lineage cells.

The Lmx1a lineage contributes to a diverse array of midline glial and neuronal populations, making it challenging to determine the role of the extent of the Lmx1a-lineage-derived neurons in the CC crossing phenotype in *Ctnnb1* LOF and GOF mice. Selective targeting of the neuronal midline guidance cells, either via a suitable Cre line or by *in utero* electroporation, may resolve the role of CTNNB1 in these cells.

RESOURCE AVAILABILITY

Lead contact

Requests for further information and resources should be directed to and will be fulfilled by the lead contact, Prof. Shubha Tole (stole@tifr.res.in).

Materials availability

This study did not generate new unique reagents. Three out of the four transgenic mouse strains used are commercially available from The Jackson Laboratory and are listed in the key resources table.

Data and code availability

This paper analyzes existing, publicly available single-cell RNA sequencing (scRNA-seq) dataset, accessible at (Loo et al., 2019,[15] GSE123335). The GSE accession number is listed in the key resources table. Imaging data reported in this paper will be shared by the lead contact upon request.

Standard Seurat analysis pipeline was used for the analysis of the single cell data. This paper does not report original code.

All raw data, experimental and analysis method, and original images supporting the findings of this study are available from the corresponding author upon reasonable request. Any additional information required to reanalyze the data reported in this paper is available from the lead contact upon request.

ACKNOWLEDGMENTS

We thank the parents of the five CTNNB1 syndrome patients for their active cooperation and for sharing information. We thank Dr. K. Millen (Seattle Children's Hospital) for the kind gift of the Lmx1aCre line, Raj Awatramani (Department of Neurology and Center for Genetic Medicine, Northwestern University Feinberg Medical School Chicago, Illinois; β-catenin exon 2–6 floxed mice described in Brault et al.[13]), and Prof. Makoto M. Taketo (Kyoto University, Kyoto; *Ctnnb1* exon 3 floxed mice). We thank Dr. Shital Suryavanshi and the animal house staff of the Tata Institute of Fundamental Research (TIFR) for their invaluable support. We thank Adityo Chaudhury (TIFR) for his help in harvesting embryos for the revised submission. Funding: Department of Atomic Energy, Govt. of India (Project Identification no. RTI4003, DAE OM no. 1303/2/2019/R&D-II/DAE/2079) (S.T.), Council of Scientific & Industrial Research, Govt. of India (Project Identification no. CSIR OLP002505, OLP242505, HCP0047) (A.P.), and the Slovenian Research and Innovation Agency under grant J7-4537 (D.O.).

AUTHOR CONTRIBUTIONS

Conceptualization, A.P. and S.T.; validation, A.P., D.D., A.S., and S.Y.; formal analysis, A.P., D.O., D.D., and A.S.; investigation, A.P., D.D., D.O., S.M., D.G., N.J., A.S., M.B., V.S., I.T., and S.Y.; writing—original draft, A.P. and S.T.; writing—review and editing, A.P., A.S., and S.T.; visualization, A.P., D.D., A. S., and S.T.; supervision, S.T.; project administration, S.T.; funding acquisition, S.T., D.O., and A.P.

DECLARATION OF INTERESTS

All the authors declare no competing interests.

DECLARATION OF GENERATIVE AI AND AI-ASSISTED TECHNOLOGIES IN THE WRITING PROCESS

All the authors declare that AI and AI-assisted technologies were not used for manuscript preparation.

STAR★METHODS

Detailed methods are provided in the online version of this paper and include the following:

- KEY RESOURCES TABLE
- EXPERIMENTAL MODEL AND STUDY PARTICIPANT DETAILS
  - Human data collection
  - Animal maintenance and genotyping
- METHOD DETAILS
  - Tissue sections and immunohistochemistry
  - In-situ hybridization
  - Image acquisition and analysis
  - Analysis of published scRNA-seq dataset
- QUANTIFICATION AND STATISTICAL ANALYSIS
  - Image analysis
  - Statistical tests

SUPPLEMENTAL INFORMATION

Supplemental information can be found online at https://doi.org/10.1016/j.isci.2025.113335.

Received: October 23, 2024
Revised: July 15, 2025
Accepted: August 7, 2025
Published: August 9, 2025

REFERENCES

1. Suárez, R., Gobius, H., and Richards, L.J. (2014). Evolution and development of interhemispheric connections in the vertebrate forebrain. Front. Hum. Neurosci. *8*, 497.
2. Gavrish, M., Kustova, A., Celis Suescún, J.C., Bessa, P., Mitina, N., and Tarabykin, V. (2023). Molecular mechanisms of corpus callosum development: a four-step journey. Front. Neuroanat. *17*, 1276325. https://doi.org/10.3389/fnana.2023.1276325.
3. Shu, T., and Richards, L.J. (2001). Cortical Axon Guidance by the Glial Wedge during the Development of the Corpus Callosum. J. Neurosci. *21*, 2749–2758.
4. Shu, T., Li, Y., Keller, A., and Richards, L.J. (2003). The glial sling is a migratory population of developing neurons. Development *130*, 2929–2937.
5. Shu, T., Butz, K.G., Plachez, C., Gronostajski, R.M., and Richards, L.J. (2003). Abnormal Development of Forebrain Midline Glia and Commissural Projections in Nfia Knock-Out Mice. J. Neurosci. *23*, 203–212.
6. Shu, T., Puche, A.C., and Richards, L.J. (2003). Development of midline glial populations at the corticoseptal boundary. J. Neurobiol. *57*, 81–94.
7. Niquille, M., Garel, S., Mann, F., Hornung, J.P., Otsmane, B., Chevalley, S., Parras, C., Guillemot, F., Gaspar, P., Yanagawa, Y., and Lebrand, C. (2009). Transient neuronal populations are required to guide callosal axons: A role for semaphorin 3C. PLoS Biol. *7*, e1000230.
8. Wegiel, J., Flory, M., Kaczmarski, W., Brown, W.T., Chadman, K., Wisniewski, T., Nowicki, K., Kuchna, I., Ma, S.Y., and Wegiel, J. (2017). Partial agenesis and hypoplasia of the corpus callosum in idiopathic autism. J. Neuropathol. Exp. Neurol. *76*, 225–237.
9. Gumbiner, B.M. (2005). Regulation of cadherin-mediated adhesion in morphogenesis. Nat. Rev. Mol. Cell Biol. *6*, 622–634. https://doi.org/10.1038/nrm1699.
10. Valenta, T., Hausmann, G., and Basler, K. (2012). The many faces and functions of Î 2-catenin. EMBO J. *31*, 2714–2736. https://doi.org/10.1038/emboj.2012.150.
11. Chizhikov, V.V., Lindgren, A.G., Mishima, Y., Roberts, R.W., Aldinger, K.A., Miesegaes, G.R., Currle, D.S., Monuki, E.S., and Millen, K.J. (2010). Lmx1a regulates fates and location of cells originating from the cerebellar rhombic lip and telencephalic cortical hem. Proc. Natl. Acad. Sci. USA *107*, 10725–10730.
12. Harada, N., Tamai, Y., Ishikawa, T., Sauer, B., Takaku, K., Oshima, M., and Taketo, M.M. (1999). Intestinal Polyposis in Mice with a Dominant Stable Mutation of the β-Catenin Gene. EMBO J. *18*, 5931–5942. https://www.embopress.org.
13. Brault, V., Moore, R., Kutsch, S., Ishibashi, M., Rowitch, D.H., McMahon, A.P., Sommer, L., Boussadia, O., and Kemler, R. (2001). Inactivation of the β-catenin gene by Wnt1-Cre-mediated deletion results in dramatic brain malformation and failure of craniofacial development. Development *128*, 1253–1264.
14. Parichha, A., Suresh, V., Chatterjee, M., Kshirsagar, A., Ben-Reuven, L., Olender, T., Taketo, M.M., Radosevic, V., Bobic-Rasonja, M., Trnski, S., et al. (2022). Constitutive activation of canonical Wnt signaling disrupts choroid plexus epithelial fate. Nat. Commun. *13*, 633.

15. Loo, L., Simon, J.M., Xing, L., McCoy, E.S., Niehaus, J.K., Guo, J., Anton, E.S., and Zylka, M.J. (2019). Single-cell transcriptomic analysis of mouse neocortical development. Nat. Commun. *10*, 134.

16. Machon, O., Backman, M., Machonova, O., Kozmik, Z., Vacik, T., Andersen, L., and Krauss, S. (2007). A dynamic gradient of Wnt signaling controls initiation of neurogenesis in the mammalian cortex and cellular specification in the hippocampus. Dev. Biol. *311*, 223–237.

17. Grove, E.A., Tole, S., Limon, J., Yip, L., and Ragsdale, C.W. (1998). The hem of the embryonic cerebral cortex is defined by the expression of multiple Wnt genes and is compromised in Gli3-deficient mice. Development *125*, 2315–2325.

18. Fenlon, L.R., Suarez, R., Lynton, Z., and Richards, L.J. (2021). The evolution, formation and connectivity of the anterior commissure. Semin. Cell Dev. Biol. *118*, 50–59. https://doi.org/10.1016/j.semcdb.2021.04.009.

19. Machon, O., van den Bout, C.J., Backman, M., Kemler, R., and Krauss, S. (2003). Role of β-catenin in the developing cortical and hippocampal neuroepithelium. Neuroscience *122*, 129–143.

20. Kayumi, S., Pérez-Jurado, L.A., Palomares, M., Rangu, S., Sheppard, S.E., Chung, W.K., Kruer, M.C., Kharbanda, M., Amor, D.J., McGillivray, G., et al. (2022). Genomic and phenotypic characterization of 404 individuals with neurodevelopmental disorders caused by CTNNB1 variants. Genet. Med. *24*, 2351–2366.

21. Wang, Y., Zhang, J., Mori, S., and Nathans, J. (2006). Axonal growth and guidance defects in Frizzled3 knock-out mice: A comparison of diffusion tensor magnetic resonance imaging, neurofilament staining, and genetically directed cell labeling. J. Neurosci. *26*, 355–364.

22. Keeble, T.R., Halford, M.M., Seaman, C., Kee, N., Macheda, M., Anderson, R.B., Stacker, S.A., and Cooper, H.M. (2006). The Wnt receptor Ryk is required for Wnt5a-mediated axon guidance on the contralateral side of the corpus callosum. J. Neurosci. *26*, 5840–5848.

23. Rattner, A., Terrillion, C.E., Jou, C., Kleven, T., Hu, S.F., Williams, J., Hou, Z., Aggarwal, M., Mori, S., Shin, G., et al. (2020). Developmental, cellular, and behavioral phenotypes in a mouse model of congenital hypoplasia of the dentate gyrus. eLife *9*, e62766.

24. Chai, G., Szenker-Ravi, E., Chung, C., Li, Z., Wang, L., Khatoo, M., Marshall, T., Jiang, N., Yang, X., McEvoy-Venneri, J., et al. (2021). A Human Pleiotropic Multiorgan Condition Caused by Deficient Wnt Secretion. N. Engl. J. Med. *385*, 1292–1301.

25. Lee, S., Chen, D.Y., Zaki, M.S., Maroofian, R., Houlden, H., Di Donato, N., Abdin, D., Morsy, H., Mirzaa, G.M., Dobyns, W.B., et al. (2019). Bi-allelic Loss of Human APC2, Encoding Adenomatous Polyposis Coli Protein 2, Leads to Lissencephaly, Subcortical Heterotopia, and Global Developmental Delay. Am. J. Hum. Genet. *105*, 844–853.

26. Tucci, V., Kleefstra, T., Hardy, A., Heise, I., Maggi, S., Willemsen, M.H., Hilton, H., Esapa, C., Simon, M., Buenavista, M.T., et al. (2014). Dominant β-catenin mutations cause intellectual disability with recognizable syndromic features. J. Clin. Investig. *124*, 1468–1482.

27. Magnani, D., Hasenpusch-Theil, K., Benadiba, C., Yu, T., Basson, M.A., Price, D.J., Lebrand, C., and Theil, T. (2014). Gli3 Controls Corpus Callosum Formation by Positioning Midline Guideposts During Telencephalic Patterning. Cereb. Cortex *24*, 186–198.

28. Borrelli, C., Valenta, T., Handler, K., Vélez, K., Gurtner, A., Moro, G., Lafzi, A., Roditi, L.d.V., Hausmann, G., Arnold, I.C., et al. (2021). Differential regulation of β-catenin-mediated transcription via N- and C-terminal cofactors governs identity of murine intestinal epithelial stem cells. Nat. Commun. *12*, 1368.

29. Valenta, T., Gay, M., Steiner, S., Draganova, K., Zemke, M., Hoffmans, R., Cinelli, P., Aguet, M., Sommer, L., and Basler, K. (2011). Probing transcription-specific outputs of β-catenin *in vivo*. Genes Dev. *25*, 2631–2643.

30. Fonov, V.S., Evans, A.C., McKinstry, R.C., Almli, C.R., and Collins, D.L. (2009). Unbiased nonlinear average age-appropriate brain templates from birth to adulthood. Neuroimage *47*, S102.

31. Chizhikov, V.V., and Millen, K.J. (2004). Control of roof plate formation by Lmx1a in the developing spinal cord. Development *131*, 2693–2705.

STAR★METHODS

KEY RESOURCES TABLE

REAGENT or RESOURCE	SOURCE	IDENTIFIER
Antibodies		
Mouse monoclonal anti-β-CATENIN	BD biosciences	Cat# 610153; RRID: AB_397555
Rabbit monoclonal anti-β-CATENIN	Cell Signaling Technology	Cat# 8814; RRID: AB_11127203
Rabbit polyclonal anti-RFP	Abcam	Cat# ab62341; RRID: AB_945213
Mouse monoclonal anti-RFP	Invitrogen	Cat#MA5-15257; RRID: AB_10999796
Rat monoclonal anti-L1CAM	Merk Millipore	Cat# MAB5272; RRID: AB_2133200
Rabbit polyclonal anti-GFAP	Sigma-Aldrich	Cat# G9269; RRID: AB_477035
Rabbit polyclonal anti-BLBP	Sigma Aldrich	Cat# ABN14; RRID: AB_10000325
Rabbit polyclonal anti ALDH1L1	Abcam	Cat# ab87117; RRID: AB_10712968
Rabbit monoclonal anti AQP4	Cell Signaling Technology	Cat# 59678; RRID: AB_2799571
Rabbit monoclonal anti NEUN	Abcam	Cat# 177487; RRID: AB_2532109
Rabbit monoclonal anti SOX9	Abcam	Cat# 185966; RRID: AB_2728660
Rabbit monoclonal anti LEF1	Cell Signaling Technology	Cat# 2230; RRID: AB_823558
Rabbit monoclonal anti-CALRETININ	ABclonal	Cat# A21965; N/A
Rabbit monoclonal anti-TBR1	Invitrogen	Cat# MA5-32564; RRID: AB_2809841
Goat anti-rabbit Alexa fluor 488	Invitrogen	Cat# A11034;RRID: AB_2576217
Goat anti-mouse Alexa fluor 594	Invitrogen	Cat# R37121;RRID: AB_2556549
Goat anti-rabbit Alexa fluor 568	Invitrogen	Cat# A11011 ;RRID: AB_143157
Donkey anti-rabbit Alexa fluor 647	Invitrogen	Cat# A31573; RRID: AB_2536183
Goat anti-mouse Alexa fluor 647	Invitrogen	Cat# A21236; RRID: AB_2535812
Goat anti-mouse Alexa fluor 488	Invitrogen	Cat#A28175; RRID: AB_2536161
Goat anti-rat Alexa fluor 488	Invitrogen	Cat# A11006; RRID: AB_2534074
Chemicals, peptides, and recombinant proteins		
Paraformaldehyde	Sigma	Cat# P6148
Citric acid monohydrate	Sigma	Cat# C7129
Trisodium citrate dihydrate	Sigma	Cat# S1804
Fluor Shield mounting reagent	Sigma	Cat# F6182
PAP pen	Sigma	Cat# Z672548
TritonX-100	Sigma	Cat# X100
Super Frost Plus slides	EMS	Cat# EMS 71869-10
Slide mailers	EMS	Cat# EMS 71549-08
Horse serum	Invitrogen	Cat# 16050130
anti-DIG (Digoxygenin) Fab fragments	Roche	Cat#11093274910; RRID:N/A
DAPI	Invitrogen	Cat# D1306; RRID: AB_2629482
Experimental models: Organisms/strains		
Mouse: Lmx1aCre	Gift from Prof. Kathy Millen (Centre for Integrative Brain Research, Seattle; Children's Research Institute)	RRID:IMSR_JAX:037459, Strain #:037459

(*Continued on next page*)

Continued

REAGENT or RESOURCE	SOURCE	IDENTIFIER
Mouse: β-cat flox(ex3)	Gift from Prof. Makoto M. Taketo, Kyoto University	NA
Mouse: β-cat flox(ex2-6)	Gift from Prof. Raj Awatramani (Department of Neurology and Center for Genetic Medicine, Northwestern University Feinberg Medical School Chicago, Illinois	RRID: IMSR_JAX:004152, Strain #:004152
Mouse: Ai9 reporter: B6.Cg-Gt(ROSA)26Sortm9(CAG-tdTomato)Hze/J)	JAX lab	RRID: IMSR_JAX: 007909; Strain #:007909
Oligonucleotides		
Lmx1a cDNA cloned in pBluescript Plasmid	Gift from Prof. Kathy Millen (Centre for Integrative Brain Research, Seattle; Children's Research Institute)	N/A
Cre genotyping primer (Forward) 5'ATTTGCCTGCATTACCGGTC3', (Reverse) 5'ATCAACGTTTTCTTTTCGG3;	Parichha et al., 2022[14]	N/A
β-catenin GOF (Exon 3 floxed) genotyping primer: (Forward) 5′ GCTGCGTGGACAATGGCTAC3′; (Reverse) 5′GCTTTTCTGTCCGGCTCCAT3	Harada et al., 1999[12]	N/A
β-catenin LOF (Exon 2-6 floxed) genotyping primer: RM41 (5′AAGGTAGAGTGATGAAAGTTGTT3′), RM42 (5′CACCATGTCCTCTGTCTATTC3′), RM43 (5′TACACTATTGAATCACAGGGACTT3′)	Brault et al., 2001[13]	N/A
Software and algorithms		
FIJI/Image	Schindelin et al., 2012[30]	https://imagej.net/software/fiji/
Zen blue	Zeiss	V3.4
FluoView	Olympus (Evident)	V4.2
Prism	Graph Pad	V10
CellSens	Olympus (Evident)	1.7
R studio	R	V 4.5.0
Other		
MRI data for control patients	MR image database	(Fonov, V.S. et al., 2009,[31] https://nist.mni.mcgill.ca/infant-atlases-0-4-5-years)
ScRNA-seq dataset	Loo et al., 2019[15]	GSE123335

EXPERIMENTAL MODEL AND STUDY PARTICIPANT DETAILS

Human data collection

In a prospective cohort study, performed between May 2021 and November 2022 in Slovenia, clinical data of patients carrying a mutation in the CTNNB1 gene were collected, including magnetic resonance imaging (MRI) data. This study was registered at ClinicalTrials.gov (NCT04812119), where a detailed study protocol can be found. The study was approved by the National Medical Ethics Committee of the Republic of Slovenia (0120-80/2021/4). Written informed consent was collected from all patients/parents. Five patients who are part of this cohort study and are described in this manuscript presented with abnormalities in the CC. Control age-matched MRI data displayed in Figure 1 is obtained from a publicly available MR image database (Fonov, V.S. et al., 2009, https://nist.mni.mcgill.ca/infant-atlases-0-4-5-years [30] Click or tap here to enter text.).

Animal maintenance and genotyping

The Institutional Animal Ethics Committee of the Tata Institute of Fundamental Research, Mumbai, India, approved all animal protocols used in this study. For the kind gifts of mouse lines used in this study, we thank Prof. Kathy Millen (Centre for Integrative Brain Research, Seattle Children's Research Institute; Lmx1aCre line described in Chizhikov et al.[11,31]), Prof. Raj Awatramani (Department of Neurology and Center for Genetic Medicine, Northwestern University Feinberg Medical School Chicago, Illinois; β-catenin exon

2-6 floxed mice described in Brault et al.[13]), and Prof. Makoto M. Taketo (Kyoto University, Kyoto; *Ctnnb1* exon 3 floxed mice[12]). The Ai9 reporter mouse line (Stock No. 007909) was obtained from JAX labs. All mice were maintained under ambient temperature and humidity conditions, with a strict 12-h light/dark cycle. Food and water were available *ad libitum*. The noon of the day on which the vaginal plug was observed was considered embryonic day 0.5 (E0.5). Only male embryos were analyzed in this study because the Lmx1aCre transgene is located on the X chromosome. Females display mosaic expression of the Cre due to random X inactivation and therefore display unpredictable variability in the phenotype. Controls were (male) littermates unless stated otherwise. Since germline recombination occurs in the testes of the Lmx1aCre males, the breeding colonies were maintained with the Cre transgene in female breeders. The primer sets used for genotyping were as follows:

Cre: (Forward) 5'ATTTGCCTGCATTACCGGTC3',
(Reverse) 5'ATCAACGTTTTCTTTTCGG3;

350-bp band observed in Cre-positive animals.
β-catenin GOF (Exon 3 floxed):

(Forward) 5′ GCTGCGTGGACAATGGCTAC3′;
(Reverse) 5′GCTTTTCTGTCCGGCTCCAT3′;

550-bp band for the conditional allele and 350-bp band for the wild-type allele.
β-catenin LOF (Exon 2-6 floxed): The following primer combination was used:

RM41 (5′AAGGTAGAGTGATGAAAGTTGTT3′), RM42 (5′CACCATGTCCTCTGTCTATTC3′), RM43 (5′TACACTATTGAATCACAG GGACTT3′) was used (Brault et al.[13]).

This PCR results in a wild-type band at 221 bp and a floxed band at 324 bp.

METHOD DETAILS

Tissue sections and immunohistochemistry

Mouse embryo dissections were performed in ice-cold 1x PBS. Brains were fixed in 4% PFA overnight at 4°C and equilibrated in 30% sucrose in PBS before sectioning at 25-μm thickness. Coronal sections mounted on a superfrost plus slide (catalog number: 71869-10) were transferred to a slide mailer (catalog number: EMS 71549-08) and washed with PBS $^{+}$ 0.01% TritonX-100 for 10 min, followed by two 5-min washes with PBS^{+} 0.03% TritonX-100. Antigen retrieval was performed by boiling sections in a 10 mM sodium citrate buffer (pH = 6) at 90°C for 10 min in a water bath. After cooling to room temperature (25C), slides were washed with 1x PBS^{+} 0.01% TritonX-100 for 10 min. A blocking solution of 5% heat-inactivated horse serum (catalog number 16050130 Invitrogen) in PBS^{+} 0.1% TritonX-100 was added to the slides, and they were incubated for 1 hour in a humidified chamber. This was followed by overnight incubation with the primary antibody at 4°C. On the next day, the slides were washed three times in 1x PBS $^{+}$ 0.1% TritonX-100 and then incubated with secondary antibodies at room temperature in a humidified chamber covered with aluminum foil (to prevent fluorophore bleaching). After three washes with 1x PBS for 5 min, each slide was incubated with DAPI solution for 10 min to stain the nuclei. Finally, the slides were mounted using Fluoroshield mounting medium (Sigma catalog #F6182). The primary antibodies used were as follows: anti-β-catenin (mouse, 1:200, BDbiosciences catalog #610153), anti-β-catenin (rabbit, 1:50, CST catalog # 8814), anti-RFP (rabbit, 1:200, Abcam catalog #ab62341), anti-RFP (mouse, 1:200, Invitrogen catalog #MA5-15257), anti-L1CAM (rabbit, 1:200, Merk Millipore, catalog #MAB5272), anti-GFAP (rabbit, 1:200, Sigma-Aldrich, catalog # G9269), and anti-BIBP (rabbit, 1:200, Sigma Aldrich, catalog # ABN14), Aldh1l1 (rabbit, 1:200, Abcam, catalog # ab87117), Aqp4 (rabbit, 1:200, CST, catalog # 59678), NeuN (rabbit, 1:500, Abcam, catalog # 177487), Sox9 (rabbit, 1:200, Abcam, catalog # 185966), Tbr1 (rabbit, 1:200, Invitrogen, catalog # MA5-32564), Calretinin (rabbit, 1:200, Abclonal, catalog # A21965). The secondary antibodies used were as follows: Goat anti-rabbit Alexa fluor 488 (1:200, Invitrogen catalog #A11034), Goat anti-mouse Alexa fluor 594 (1:200, Invitrogen catalog #R37121), Goat anti-rabbit Alexa fluor 568 (1:200, Invitrogen catalog #A11011), Donkey anti-rabbit Alexa fluor 647 (1:200, Invitrogen catalog #A31573), Goat anti-mouse Alexa fluor 647 (1:200, Invitrogen catalog #A21236), Goat anti-mouse Alexa fluor 488 (1:200, Invitrogen catalog #A28175), and Goat anti-rat Alexa fluor 488 (1:200, Invitrogen catalog #A11006).

In-situ hybridization

Plasmid for the generation of Lmx1a riboprobe was generously provided by Prof. Kathleen Millen. Mouse embryonic brain at E13.5 was fixed and cryo-sectioned using a Leica SM2000R sliding microtome at a thickness of 20 μm. Sections were mounted on Super frost Plus slides (EMS, Cat. #71869-11), followed by post fixation in 4% paraformaldehyde (PFA) for 15 minutes. After three PBS washes, tissue was treated with proteinase-K (1 μg/ml) prepared in Tris-EDTA buffer. A second post fixation step was carried out using 4% PFA for another 15 minutes, followed by additional PBS washes. Hybridization was conducted overnight (16 hours) at 70 °C in a buffer composed of 50% formamide, 2X SSC, and 1% SDS. DIG-labeled complementary RNA probes, transcribed *in vitro* from linearized plasmid templates, were used for hybridization. Templates were prepared via restriction enzyme digestion

of the plasmids. Post-hybridization, three high-stringency washes (each 45 minutes) were performed in a solution containing 50%-formamide, 2X SSC, and 1% SDS, followed by washes in 2X SSC and 0.2X SSC. For detection of signal, sections were blocked for one hour in TBST (Tris-buffered saline with 0.1% Tween-20, pH 7.5) supplemented with 10% horse serum. Sections were then incubated overnight at 4 °C with Fab fragments of anti-DIG alkaline phosphatase-conjugated antibody (Roche, Cat. #12486523) diluted 1:5000 in blocking buffer. Signal was visualized using the NBT/BCIP substrate system (Roche: NBT, Cat. #70210625; BCIP, Cat. #70251721). Sections were counterstained with nuclear Fast Red (Sigma-Aldrich, Cat. #N3020), air-dried, and cover slipped using DPX mounting medium (SDFCL, Cat. #46029).

Image acquisition and analysis

Bright-field images were acquired using a Zeiss Axioskop-5 plus microscope equipped with a Zeiss Axiocam 506 color camera and associated Zen blue (V3.4) software. Mouse sections were imaged using an Olympus FluoView 1200 & 4000 confocal microscope with FluoView software. Image analysis was performed using Fiji (ImageJ) software and Adobe Photoshop CS6.

Analysis of published scRNA-seq dataset

A published P0 mouse embryonic scRNA-seq dataset (Loo et al., 2019, GSE123335) was used for the analysis. The aligned feature-barcode matrices were downloaded from NCBI Gene Expression Omnibus and analyzed with the Seurat (v5.0.1) R package. Cells with fewer than 500 or more than 5000 genes, or with more than 10 percent mitochondrial reads were filtered out. The feature expression measurements for each cell were normalized by the total expression, multiplied by the default scale factor of 10000, and log-transformed. Principal Component Analysis (PCA) was run on the data using the top 2000 variable features to reduce dimensionality. tSNE was run on the data using the top 50 principal components for visualization purposes. The original annotations by the authors of the dataset were used to annotate cell types, and cells annotated as ‘‘Astrocytes’’ were used for the exploration of glial markers.

QUANTIFICATION AND STATISTICAL ANALYSIS

Image analysis

For Figure 1G; Figures S2B and S2C, images were acquired in tile scan mode, and stitching was performed in the Zen blue software (V3.4). For all figures, three coronal sections per brain (each 25 μm thick) were analyzed for E18.5 and P0 brains, spaced 100 μm apart along the rostrocaudal axis. For E15.5 and E13.5 brains, two rostrocaudal levels per brain were analyzed. For the quantification of corpus callosum (CC) thickness in the midline (Figures 1E and 1F), the "Line Tool" in Fiji was used. A line was drawn along the midline region of the CC, and thickness was measured using the "Measure" option in Fiji. 2 representative rostro-caudal levels were quantified, which are 100 μm apart from each other in the rostrocaudal axis (depth information shown in Figure S2. For all cell counting analyses (Figure 2), the "Cell Counter" plugin in Fiji was utilized. Cell counts were performed on stitched high-magnification, 10 μm thick stacked confocal images. Cells positive for both the marker and Ai9 were classified as type 1, while cells positive only for the marker were designated as type 2. During scrolling through the Z-stack, the "Show All" option was enabled in the plugin to prevent duplicate counting of the same cell across different Z planes. Cells that are overlapping and not clearly distinguishable were not scored. For the colocalization plot in Figure S3, the colocalization finder plugin in FIJI was used. Individual red and green channel was used to generate the plot using this plugin. For image representation, the ‘‘Z stacked’’ vs ‘‘single representative plane’’ is properly mentioned in each figure legend. Nonlinear operations such as gamma correction were not performed for any of the figures. Brightness and contrast adjustments were performed identically for control, GOF, and LOF brains. Image stitching was performed in Figures 1, 2N, and 2Q; Figures S2B, S2C, S3, S8A, and S8C. All schematics were prepared using Microsoft PowerPoint 2016 and Adobe Photoshop 2017.

Statistical tests

Biological replicates (N) were samples obtained from individual embryos/Pups. Blinded analysis was not possible for Lmx1aCre genotypes since they are easily distinguishable owing to the dramatic difference in phenotype. Statistical analyses were performed using GraphPad Prism (v9.3.1). Exact information about statistical tests and p-values are provided in the corresponding figure legends. For all statistical tests, the confidence interval selected was 95% (α=0.05). Outlier removal was not performed for any test. For all the scattered plots and bar graphs, error bars represent the SEM.